PHYSICAL REVIEW B **94**, 024503 (2016)

Strong correlations between vacancy and magnetic ordering in superconducting $K_{0.8}Fe_{2-y}Se_2$

J. Yang,[1] C. Duan,[1] Q. Huang,[2] C. Brown,[2] J. Neuefeind,[3] and Despina Louca[1,*]
[1] *University of Virginia, Charlottesville, Virginia 22904, USA*
[2] *NIST Center for Neutron Research, Gaithersburg, Maryland 20899, USA*
[3] *Oak Ridge National Laboratory, Oak Ridge, Tennessee 37831, USA*

(Received 16 November 2015; revised manuscript received 7 June 2016; published 5 July 2016)

The coexistence of magnetic and nonmagnetic phases in the superconducting potassium iron selenide, $K_xFe_{2-y}Se_2$, has been intensely debated. With superconductivity proposed to appear in a stoichiometric, nonmagnetic phase with *I4/mmm* crystal symmetry, the proposed nonsuperconducting phase is magnetic and has a lower symmetry, *I4/m*. The latter consists of Fe vacancies that go through a disordered-to-ordered transition in which the partially filled Fe sites create a supercell upon ordering. We show, using neutron scattering on the optimally doped composition, $K_{0.8}Fe_{2-y}Se_2$, that the absence of magnetism does not signal the presence of superconductivity. Moreover, the degree of vacancy order is coupled to the strength of the magnetic order. Superconductivity coincides with the presence of the magnetic order parameter, albeit the latter is significantly weaker than previously reported, contradicting the current understanding of this ∼ 30 K superconductor.

DOI: 10.1103/PhysRevB.94.024503

I. INTRODUCTION

When potassium, K, is intercalated between the tetrahedral layers of the binary chalcogenide superconductor, $Fe_{1-y}Se$ ($T_C \sim 8$ K), the superconducting transition temperature, T_C, shows a fourfold increase [1–7]. The $K_xFe_{2-y}Se_2$ phase diagram is quite complex. Vacancies are present at the K and Fe sites, while the latter undergoes a disorder-to-order transition at $T_S \sim 580$ K [2] upon cooling. Above this temperature, the symmetry is *I4/mmm* in which only one Fe site is present and the Fe vacancies are randomly distributed in the lattice. What happens to the lattice below T_S has been quite controversial, with several scenarios proposed. It has been suggested that a stoichiometric phase with *I4/mmm* high-temperature symmetry persists below T_S concomitantly with the emergence of a nonstoichiometric phase with a lower symmetry, *I4/m*, in which the Fe vacancies undergo long-range order. The latter crystal structure is shown in Fig. 1(a), while the *I4/mmm* symmetry is the same as that found in the $BaFe_2As_2$ Fe-based superconductor. Also reported is the possibility of a structural transition to the new vacancy-ordered state, without the presence of the *I4/mmm* high-temperature phase [3,8–11]. Moreover, an antiferromagnetic transition occurs following the structural one at $T_N \sim 560$ K [7]. Superconductivity appears in a narrow range of K intercalation, in a phase that was previously proposed to exhibit a large magnetic moment, over $3\mu_B$/Fe atom, a nontrivial quantity, and much larger than what is found in other Fe-based compounds [3]. Long-standing issues in this system have been whether or not such strong magnetic coupling is viable in the superconducting state and whether competing interactions lead to phase separation of superconducting nonmagnetic from nonsuperconducting magnetic domains [4,12–20].

At the center of the problem is the distribution of Fe vacancies and magnetic moments because of their possible role in the superconducting mechanism [21–28]. Several superlattice structures have been proposed for the long-range order of Fe vacancies, including the $\sqrt{5} \times \sqrt{5} \times 1$ [2,3,8,29] (referred to as the "245" structure), $\sqrt{2} \times \sqrt{2} \times 1$ [2,10], $\sqrt{2} \times 2\sqrt{2} \times 1$ [2,7,30], and $\sqrt{8} \times \sqrt{10} \times 1$ [4] types. Does the superconducting state appear in a minority phase devoid of a superlattice structure, as suggested from scanning tunneling [21], nuclear magnetic resonance [31], and transmission electron microscopy [7] measurements? If a stoichiometric KFe_2Se_2 (122 composition) is phase separated from the vacancy-ordered matrix, however, it implies a superconductive phase that is heavily electron doped [4,21,32,33]. Theoretical calculations have shown that in the 245 $K_xFe_{2-y}Se_2$ structure, disorder can suppress the band structure reconstruction without destroying the Fermi surface, while it raises the chemical potential, eliminating the hole pockets, in agreement with ARPES results [33,34]. Thus it is hypothesized that the degree of vacancy order is strongly coupled to Cooper pair formation and scattering. To this end, the crystal structure is revisited to investigate the structure-property relationship in this Fe-based superconductor.

Via the systematic growth of single crystals of $K_{0.8}Fe_{2-y}Se_2$, we find that the distribution of Fe vacancies, the crystal structure, and its magnetism are strongly interrelated with the superconducting volume fraction. Here, four growth conditions are compared: one in which crystals are grown in sealed quartz tubes filled with Ar and slow-cooled to room temperature; another in which crystals are grown in vacuum-sealed quartz tubes and slow-cooled to room temperature; a third in which the Ar grown crystals undergo further annealing in Ar gas at 350°C and are then quenched; and a fourth in which the vacuum grown crystals are further annealed in vacuum, also at 350°C, and quenched to room temperature. Similar growth conditions have been reported in Refs. [4], [13], and [35–38].

II. SAMPLE PREPARATION AND CHARACTERIZATION

Single crystals of $K_xFe_{2-y}Se_2$ were grown by the self-flux method. First, high-purity tetragonal FeSe powders were synthesized using the solid-state reaction method. Stoichiometric quantities of iron pieces (Alfa Aesar; 99.99%) and selenium powder (Alfa Aesar; 99.999%) were weighed and sealed in

---

[*] louca@virginia.edu

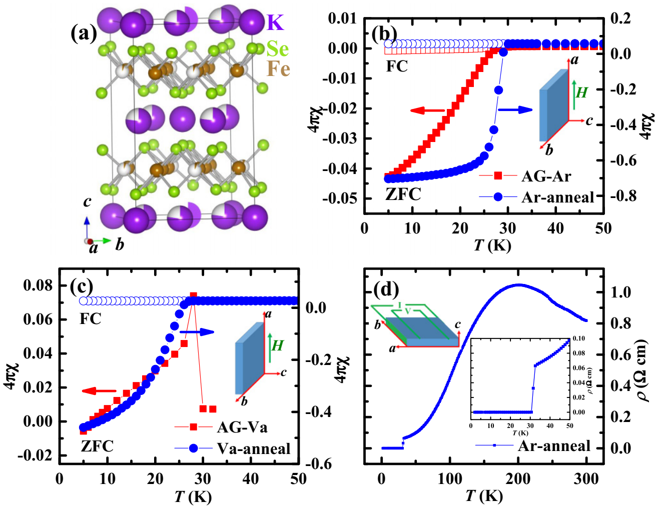

FIG. 1. (a) The *I4/m* crystal structure of $K_{0.8}Fe_{2-y}Se_2$. (b) Temperature-dependent superconducting shielding (ZFC) and Meissner (FC) fraction data for as-grown (red symbols) and annealed (blue symbols) single crystals grown in Ar gas at $H = 20$ Oe. (c) Temperature-dependent superconducting shielding (ZFC) and Meissner (FC) fraction data for the as grown (red symbols) and annealed (blue symbols) for single crystals grown in vacuum at $H = 20$ Oe. (d) Temperature-dependent resistivity for annealed (blue) single crystals grown in Ar gas. Insets: Schematics of the experimental setup.

vacuum quartz tubes. The samples were heated to 1075°C for 30 h, then annealed at 400°C for 50 h, and, finally, quenched in liquid nitrogen. K grain and FeSe powders with a nominal composition of K:FeSe = 0.8:2 were placed in an alumina crucible and double-sealed in quartz tubes partially backfilled with ultrahigh-purity argon. All weighing, mixing, grinding, and pressing procedures were performed in a glove box under an argon atmosphere with the oxygen and moisture below 1 ppm. The samples grown in vacuum were double-sealed in high-vacuum quartz tubes evacuated by a molecular pump. All samples were heated at 1030 °C for 2 h, cooled down to 750 °C at a rate of 6 °C/h, and then cooled to room temperature by switching off the power of the furnace. High-quality single crystals were mechanically cleaved from the solid chunks in the glove box. Finally, the as-grown single crystals were thermally treated for 2 h at 350°C, followed by quenching in liquid nitrogen. Single crystals grown in partially backfilled argon were thermally treated in partially backfilled argon, and single crystals grown in vacuum were thermally treated in vacuum. The actual compositions are $K_{0.74(8)}Fe_{1.70(8)}Se_2$ for the vacuum as-grown sample, $K_{0.78(4)}Fe_{1.74(5)}Se_2$ for the vacuum-annealed sample, and $K_{0.75(6)}Fe_{1.69(6)}Se_2$ for the argon-annealed sample; they were determined by inductively coupled plasma optical emission spectroscopy. The dc magnetic susceptibilities were measured using a Quantum Design PPMS in the temperature range from 2 to 300 K. Neutron powder diffraction measurements were performed using the BT1 diffractometer at the NIST Center for Neutron Research in Gaithersburg, Maryland, with the neutron wavelength of $\lambda = 2.078$ Å at 10 K. The pair density function (PDF) was determined from neutron data collected at the NOMAD diffractometer at the Spallation Neutron Source of Oak Ridge National Laboratory as a function of the temperature, from 2 to 300 K. Single crystals were ground into powder inside a helium-filled glove box prior to the experiment.

First, we describe the bulk transport and magnetization measurements. Figure 1(b) is a plot of the bulk magnetization, $4\pi\chi$, for zero-field-cooled (ZFC) and field-cooled (FC) measurements for crystals grown in Ar gas. Red squares correspond to the quenched as-grown crystals (AG-Ar), while blue circles correspond to crystals that were subsequently annealed in Ar (Ar-anneal). Figure 1(c) is a similar plot that compares the temperature dependence of $4\pi\chi$ of an as-grown crystal grown in vacuum (AG-Va; red squares) to a crystal from the same batch but with subsequent annealing in vacuum (Va-anneal;blue circles). It can readily be seen that the as-grown crystals are either marginally or not at all superconducting and show bad connectivity of the superconducting grains. On the other hand, the crystals annealed in vacuum or Ar gas show significant enhancement of the percentage diamagnetic signal. In the case of Ar-annealed crystals, it reaches close to 75% full diamagnetism, while Va-annealed crystals reach about 50%. A heat capacity measurement of as-grown samples reported in Ref. [36] shows a discontinuity at T_C, indicating that the superconductivity is bulk. Chemical analysis yielded a very similar chemical composition for the two highest-shielding-fraction crystals: a composition of $K_{0.76}Fe_{1.70}Se_2$ for the Ar-annealed and $K_{0.78}Fe_{1.74}Se_2$ for the Va-annealed crystals. For comparison, in the AG-Va crystal, which exhibits a small negative $4\pi\chi$ value at the lowest temperature, the chemical composition is $K_{0.74(8)}Fe_{1.70(8)}Se_2$. Shown in Fig. 1(d) is the resistivity, $\rho(T)$, in units of $\Omega \cdot$ cm. A broad hump indicating a semiconducting-to-metal crossover is observed around 200 K, followed by the superconducting transition at ~ 31 K [1,4]. The back-scattered electron images of scanning electron microscopy (SEM) were measured on cleaved surfaces of Ar as-grown (AG-Ar) and Ar-annealed (Ar-anneal) samples and are shown in Fig. 2. Figures 2(a) and 2(b) exhibit the results

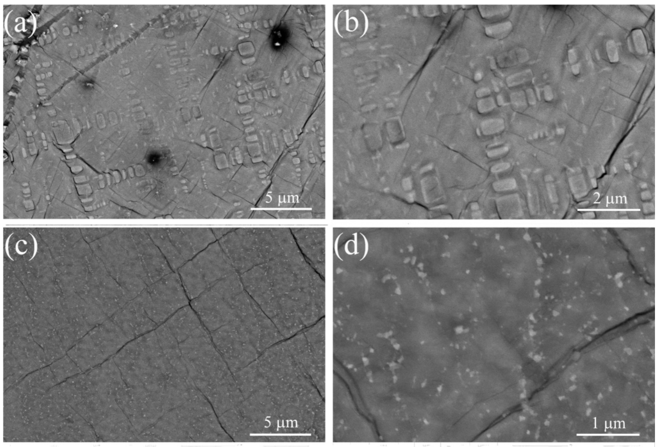

FIG. 2. Back-scattered electron images of SEM measurements on the cleaved surface of two typical samples. Topography of the cleaved surface of the Ar as-grown (AG-Ar) sample; scale bars are (a) 5 μm and (b) 2 μm. Topography of the cleaved surface of the Ar annealed sample; scale bars are (c) 5 μm and (d) 1 μm. Measurements were done at a voltage of 10 kV.

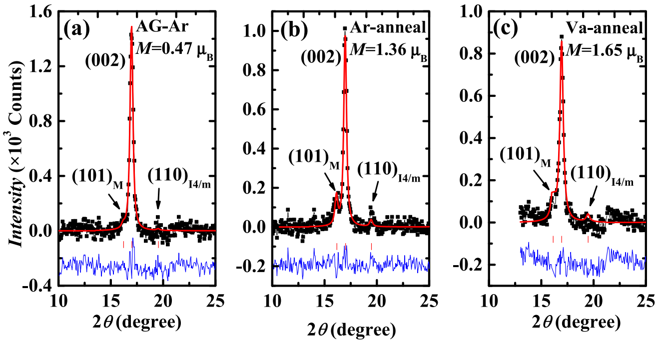

FIG. 3. Neutron diffraction data collected at BT-1 of the (002) peak at 2 K for (a) gas as grown in Ar, (b) gas annealed in Ar, and (c) gas annealed in vacuum. They are fit with *I4/m* symmetry. The three panels show the magnetic (101) and the superlattice (110) peaks that arise from *I4/m* symmetry. The magnetic moments are significantly reduced, similarly to the superlattice peak, which suggests that vacancy ordering is quite poor.

for the AG-Ar sample. Clearly the surface separates into two kinds of regions: domains with brighter color and a rectangular shape, buried in a background of darker regions. However, as shown in Figs. 2(c) and 2(d), the brighter rectangular domains were not observed in the Ar-annealed sample. Instead, very tiny bright dots were observed in the Ar-annealed sample. Furthermore, differently from previous reports that the brighter domains were changed to smaller but connecting chains in the annealed sample, we do not see obvious connecting chains on our Ar-anneal sample, even at the highest resolution as shown in Fig. 2(d). In this case, the enhancement of the superconducting shielding fraction of the Ar-annealed sample is not due to the connectivity of the minority phase. The results on the annealed crystal are somewhat different from those reported in Ref. [4].

The neutron diffraction data collected using the BT1 diffractometer at the NIST Center for Neutron Research suggest that all crystals have some magnetic component, i.e., magnetic peaks are present in all as shown in Figs. 3(a)–3(c), albeit with varying intensities and much smaller than previously reported [2,3]. The magnetic peaks can only be indexed in the *I4/m* symmetry. Moreover, the refined moments are nowhere near as large as previous reports stated [2,3]. The results from the refinement are summarized in Table I. From the data refinement, it is deduced that in the marginal superconductors, very weak magnetism is present, if any. Thus the absence of magnetism is not indicative of a superconducting state. In the plot in Fig. 2(a), the neutron diffraction pattern collected at 2 K for the AG-Ar crystal is fit using *I4/m* symmetry. The magnetic peak is barely discernible as indicated, and the magnetic moment is refined to be about $0.5 \pm 0.3\ \mu_B$. The same is true for the (110) Bragg peak, which is from the *I4/m* vacancy-ordered structure of the $\sqrt{5} \times \sqrt{5} \times 1$ type. Most important is the fact that the Fe1 and Fe2 sites are almost equally occupied as shown in Table I, with vacancies at both sites, although more at the Fe1 than at the Fe2 site. Therefore in the absence of a strong magnetic moment, both sites carry vacancies, while the very weak (110)

TABLE I. Refinement results from the Rietveld analysis for (a) AG-Ar, (b) Ar-annealed, and (c) vacuum-annealed samples. Coordinates are as follows: for K1, (0,0,0); for K2, $(x,y,0)$; for Fe1, $(0,\frac{1}{2},\frac{1}{4})$; for Fe2, $(x,y,\frac{1}{4})$; for Se1, $(\frac{1}{2},\frac{1}{2},z)$; and for Se2, (x,y,z).

		U_{iso} (Å^2)	Occupancy
	(a) AG-Ar: $a = b = 8.652$ Å, $c = 14.046$ Å, $\chi^2 = 2.278$, $wR_p = 0.057$, $R_p = 0.045$		
K1		0.020	0.756
K2	$x = 0.337$, $y = 0.199$	0.020	0.756
Fe1		0.044	0.512
Fe2	$x = 0.198$, $y = 0.095$	0.044	0.829
Se1	$z = 0.144$	0.006	1.000
Se2	$x = 0.122$, $y = 0.318$, $z = 0.145$	0.006	1.000
	(b) Ar annealed: $a = b = 8.671$ Å, $c = 14.029$ Å, $\chi^2 = 1.304$, $wR_p = 0.060$, $R_p = 0.047$		
K1		0.020	0.835
K2	$x = 0.337$, $y = 0.199$	0.020	0.835
Fe1		0.029	0.350
Fe2	$x = 0.198$, $y = 0.095$	0.029	1.000
Se1	$z = 0.144$	0.010	1.000
Se2	$x = 0.122$, $y = 0.318$, $z = 0.145$	0.010	1.000
	(c) Vacuum annealed: $a = b = 8.648$ Å, $c = 14.029$ Å, $\chi^2 = 2.139$, $wR_p = 0.069$, $R_p = 0.054$		
K1		0.020	0.836
K2	$x = 0.337$, $y = 0.199$	0.020	0.836
Fe1		0.020	0.528
Fe2	$x = 0.198$, $y = 0.095$	0.020	1.000
Se1	$z = 0.144$	0.004	1.000
Se2	$x = 0.122$, $y = 0.318$, $z = 0.145$	0.004	1.000

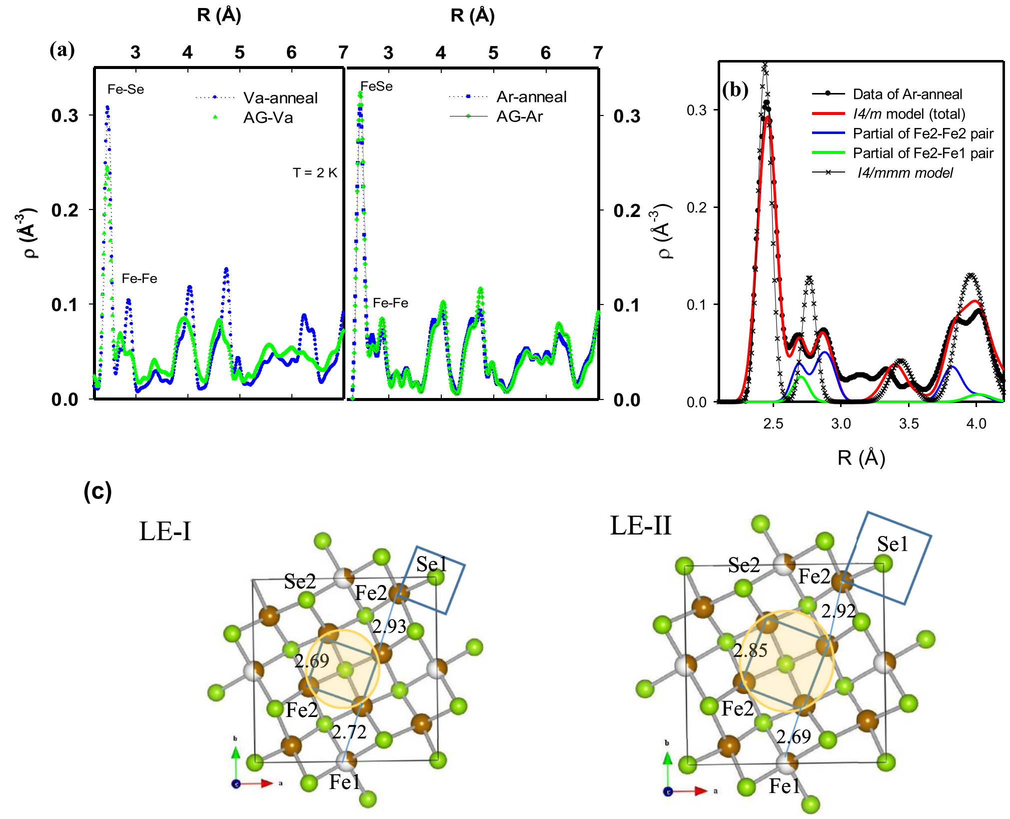

FIG. 4. (a) Data PDFs corresponding to the local atomic structure for the four crystals are shown. (b) Data for the Ar-annealed crystal are fit to a local model assuming *I4/m* symmetry. The parameters for this model are provided in Table II. Also included in the model is an excess of about 5% pure Fe metal, a residual from the synthesis. The fitting between the experimental data and the model is quite good, especially in the region involving Fe correlations between 2.5 and 3.0 Å. Also shown are the partial functions calculated from the model for the two most significant correlations of Fe: Fe2-Fe2 and Fe2-Fe1. Also shown, by the dashed line, is a model assuming a local structure based on *I4/mmm* symmetry. The single Fe-Fe correlation is present in this symmetry, which resides in between the Fe correlations observed in the experimental data. (c) Real-space image of the Fe sublattice, projected on the *ab* plane, which corresponds to the PDF shown in (b).

peak signifies poor vacancy ordering because the occupancy of the Fe1 and Fe2 sites is comparable. Moreover, when the Fe2 site is only partially full, superconductivity is suppressed.

With annealing, the Fe2 site occupancy reaches unity, while the Fe1 site remains partially empty. Further, with the increase in the occupancy at the Fe2 site, the magnetic moment increases as well. This is because the magnetism is associated with the Fe2 site and not with the Fe1 site [3,39,40]. The neutron data from the Ar-annealed crystal in Fig. 3(b) clearly show more intense $(101)_M$ and $(110)_{I4/m}$ peaks than in the AG-Ar. In this case, the magnetic moment is refined to be $\sim 1.36 \pm 0.07\,\mu_B$. Similarly, in the Va-anneal crystal, the magnetic moment is comparable, at $\sim 1.65 \pm 0.16\,\mu_B$. However, the fraction of Fe1 site occupancy is higher in the latter compound than in the Ar-annealed crystal, which explains the reduction of its $(110)_{I4/m}$ superlattice peak due to fewer vacancies [Fig. 3(c)]. In comparison to earlier neutron measurements [3], the magnetic moment is significantly smaller and so is the superlattice peak of $(110)_{I4/m}$ from the vacancy ordering. This is because the Fe1 site is not as sparsely populated as in Ref. [3], hence there is a lower degree of vacancy ordering overall in our crystals, which most likely reduces scattering and promotes superconductivity. Thus, enhancement of the superconducting connectivity is related to the higher occupancy of the Fe2 site, reduction of the degree of vacancy ordering, and suppression of the magnetic moment.

The subtleties of the Fe distribution between the two sites can also be seen in the local structure, obtained by Fourier transforming the diffraction data collected using the high-intensity powder diffractometer, NOMAD, at Oak Ridge National Laboratory. Represented by the PDF, $\rho(r)$, the local atomic structure is a superposition of the atomic correlations regardless of symmetry or periodicity [41]. The PDFs shown in Fig. 4(a) are from data collected on the same crystals. The first peak corresponds to Fe-Se correlations within the tetrahedron, which is the shortest bond in the unit cell, while the second corresponds to Fe-Fe correlations as reported elsewhere [39,42]. The fluctuations of $\rho(r)$ correspond to local atomic variations present in the different crystals, with clear differences observed between the samples prepared in vacuum (left panel) and those prepared in Ar gas (right panel). The Fe-Fe double-peak feature present in all compounds cannot be reproduced by a model PDF calculated based on *I4/mmm* symmetry [39] and shown as the dashed line in Fig. 4(b).

The best fit to the local environment (LE) is obtained when *I4/m* symmetry is assumed. Given that within *I4/m* there are two Fe sites, three kinds of bond pairs contribute to the Fe

TABLE II. Unit cell parameters for the two local environments (LE-I and LE-II) in $K_{0.8}Fe_{2-y}Se_2$ that can describe the Fe-Fe correlations in the local lattice of an Ar-annealed sample.

	LE-I: $a = 8.6929$ Å, $c = 14.016$ Å				LE-II: $a = 8.8389$ Å, $c = 13.89$ Å			
	x	*y*	*z*	Occupancy	*x*	*y*	*z*	Occupancy
K1	0	0	0	0.835	0	0	0	0.835
K2	0.3995	0.197	0	0.835	0.404	0.178	0	0.835
Fe1	0	0.5	0.25	0.35	0	0.5	0.25	0.35
Fe2	0.2	0.089	0.2508	1	0.209	0.09	0.2508	1
Se1	0.5	0.5	0.145	1	0.5	0.5	0.145	1
Se2	0.1147	0.294	0.142	1	0.115	0.294	0.142	1

correlation peak, from Fe1-Fe1, Fe1-Fe2, and Fe2-Fe2. The presence of short and long Fe-Fe bonds in the region from 2.6 to 3.0 Å is from the superposition of the three pairs. The multiplicity at the Fe2 site is 16, while at the Fe1 site it is 4; thus the area under the two peaks is scaled proportionately. To contrast with the *I4/mmm* symmetry in which only one Fe site is present, with an Fe-Fe bond length of ∼ 2.8 Å as shown in Fig. 4(b), the double-peak feature observed in the data for all samples is a signature of *I4/m*. This analysis cannot exclude the possibility of the presence of small quantities (less than 5%) of the *I4/mmm* structure. Note that the weight distribution between the double-peak feature is different from crystal to crystal, which is a reflection of the different Fe and K distributions and the Fe vacancies, as discussed above. At the same time, the susceptibility data in Fig. 1 show clear differences between samples that have been annealed and those that have not. Thus one would expect that if a stoichiometric *I4/mmm* associated with superconductivity phase separates, it would become more prominent in the annealed samples. Instead, what is observed is a redistribution of the Fe bonds within the same symmetry. This is discussed next.

The local geometry is governed by the K2, Fe2, and Se1/2 coordinates, while the Fe1 and K1 coordinates are fixed by the *I4/m* symmetry. The initial atom parameters used to calculate a local model are obtained from the crystal refinement. These values are subsequently modified to best fit the $\rho(r)$. The parameters are listed in Table II. The results from the fitting are shown in Fig. 4(b) where the data (black circles) for the Ar-annealed sample are compared to a local model (solid red line). In this model, a double unit cell is assumed, with two local Fe2 environments. The two environments are shown in Fig. 4(c) in plots of the FeSe sublattice projected on the *ab* plane. The square plaquette at the center of each unit is contracted in the local environment LE-I and expanded in LE-II, resulting in two unique environments as shown in the figure. The superposition of the two unit cells results in an overall fitting that is the red solid line in Fig. 4(b). The model, which also includes 5% excess Fe, can fit the data well, especially in the region of the Fe correlations. Similar models have been obtained for the other samples as well. Also shown in this figure are the partial functions calculated from this model for the Fe2-Fe2 and Fe2-Fe1 correlations, which show the distribution of the bonds. Note that the bonds between Fe1 and Fe1 atoms do not contribute in this region at all. The presence of the two LEs around Fe may be related to the number of Fe1 vacancies in the immediate vicinity. As the ratio of LE-I to LE-II changes from sample to sample, so does the distribution of vacancies, which in turn affects the connectivity between the superconducting regions.

In summary, the complex lattice landscape resulting from competing magnetic and superconducting phases is a phenomenon commonly observed in complex superconducting systems such as cuprates, bismuth perovskites, cobaltates, and, more recently, H_2S. The complex local structure of $K_xFe_{2-y}Se_2$ is manipulated by varying the growth conditions, with the result of producing different phases leading to different responses. The distribution of Fe, its magnetism, and the vacancies are strongly related to the connectivity of the superconducting grains with annealing. The Fe environment sensitively reflects the emergent complexity in this class of Fe-based superconductors.

ACKNOWLEDGMENTS

The authors would like to acknowledge valuable discussions with W. Bao, T. Egami, A. Bianconi, and W. Ku. The work at the University of Virginia was supported by the U.S. Department of Energy, Office of Basic Energy Sciences under Contract No. DE-FG02-01ER45927, and that at Oak Ridge National Laboratory, by the Office of Basic Energy Sciences, Division of Scientific User Facilities. The work at NIST was supported by the US Department of Commerce.

---

[1] J. Guo, S. Jin, G. Wang, S. Wang, K. Zhu, T. Zhou, M. He, and X. Chen, Phys. Rev. B **82**, 180520(R) (2010).

[2] W. Bao, G. Li, Q. Huang, G. Chen, J. He, D. Wang, M. A. Green, Y. Qiu, J. Luo, and M. Wu, Chin. Phys. Lett. **30**, 027402 (2013).

[3] W. Bao, Q. Huang, G. Chen, M. A. Green, D. Wang, J. He, and Y. Qiu, Chin. Phys. Lett. **28**, 086104 (2011).

[4] X. Ding, D. Fang, Z. Wang, H. Yang, J. Liu, Q. Deng, G. Ma, C. Meng, Y. Hu, and H.-H. Wen, Nat. Commun. **4**, 1894 (2013).

[5] J. J. Ying, X. F. Wang, X. G. Luo, A. F. Wang, M. Zhang, Y. J. Yan, Z. J. Xiang, R. H. Liu, P. Cheng, G. J. Ye, and X. H. Chen, Phys. Rev. B **83**, 212502 (2011).

[6] D. M. Wang, J. B. He, T. L. Xia, and G. F. Chen, Phys. Rev. B **83**, 132502 (2011).

[7] Y. J. Yan, M. Zhang, A. F. Wang, J. J. Ying, Z. Y. Li, W. Qin, X. G. Luo, J. Q. Li, J. Hu, and X. H. Chen, Sci. Rep. **2**, 212 (2012).

[8] F. Ye, S. Chi, Wei Bao, X. F. Wang, J. J. Ying, X. H. Chen, H. D. Wang, C. H. Dong, and M. Fang, Phys. Rev. Lett. **107**, 137003 (2011).

[9] M.-H. Fang, H.-D. Wang, C.-H. Dong, Z.-J. Li, C.-M. Feng, J. Chen, and H. Q. Yuan, Europhys. Lett. **94**, 27009 (2011).

[10] Z. Wang, Y. J. Song, H. L. Shi, Z. W. Wang, Z. Chen, H. F. Tian, G. F. Chen, J. G. Guo, H. X. Yang, and J. Q. Li, Phys. Rev. B **83**, 140505(R) (2011).

[11] A. Ricci, N. Poccia, G. Campi, B. Joseph, G. Arrighetti, L. Barba, M. Reynolds, M. Burghammer, H. Takeya, Y. Mizuguchi, Y. Takano, M. Colapietro, N. L. Saini, and A. Bianconi, Phys. Rev. B **84**, 060511(R) (2011).

[12] P. Dai, J. Hu, and E. Dagotto, Nature Phys. **8**, 709 (2012).

[13] Y. Liu, Q. Xing, K. W. Dennis, R. W. McCallum, and T. A. Lograsso, Phys. Rev. B **86**, 144507 (2012).

[14] L. Xie, Y. W. Yin, M. L. Teng, T. S. Su, X. G. Li, and J. Q. Li, Appl. Phys. Lett. **102**, 182601 (2013).

[15] Z.-W. Wang, Z. Wang, Y.-J. Song, C. Ma, Y. Cai, Z. Chen, H.-F. Tian, H.-X. Yang, G.-F. Chen, and J.-Q. Li, J. Phys. Chem. C **116**, 17847 (2012).

[16] S. Landsgesell, D. Abou-Ras, T. Wolf, D. Alber, and K. Prokeš, Phys. Rev. B **86**, 224502 (2012).

[17] Y. Liu, Q. Xing, W. E. Straszheim, J. Marshman, P. Pedersen, R. McLaughlin, and T. A. Lograsso, Phys. Rev. B **93**, 064509 (2016).

[18] K. Wang, H. Ryu, E. Kampert, M. Uhlarz, J. Warren, J. Wosnitza, and C. Petrovic, Phys. Rev. X **4**, 031018 (2014).

[19] R. H. Yuan, T. Dong, Y. J. Song, P. Zheng, G. F. Chen, J. P. Hu, J. Q. Li, and N. L. Wang, Sci. Rep. **2**, 00221 (2012).

[20] M. Tanaka, Y. Yanagisawa, S. J. Denholme, M. Fujioka, S. Funahashi, Y. Matsushita, N. Ishizawa, T. Yamaguchi, H. Takeya, and Y. Takano, J. Phys. Soc. Jpn. **85**, 044710 (2016).

[21] W. Li, H. Ding, P. Deng, K. Chang, C. Song, Ke He, L. Wang, X. Ma, J.-P. Hu, X. Chen, and Q.-K. Xue, Nature Phys. **8**, 126 (2012).

[22] A. Chubukov, Annu. Rev. Condens. Matter Phys. **3**, 57 (2012).

[23] J. Paglione and R. L. Greene, Nature Phys. **6**, 645 (2010).

[24] I. I. Mazin, Nature **464**, 183 (2010).

[25] K. Kuroki, S. Onari, R. Arita, H. Usui, Y. Tanaka, H. Kontani, and H. Aoki, Phys. Rev. Lett. **101**, 087004 (2008).

[26] P. J. Hirschfeld, M. M. Korshunov, and I. I. Mazin, Rep. Prog. Phys. **74**, 124508 (2011).

[27] C. De la Cruz, Q. Huang, J. W. Lynn, J. Li, W. Ratcliff, J. L. Zarestky, H. A. Mook, G. F. Chen, J. L. Luo, N. L. Wang, and P. Dai, Nature **453**, 899 (2008).

[28] Q. Huang, Y. Qiu, W. Bao, M. A. Green, J. W. Lynn, Y. C. Gasparovic, T. Wu, G. Wu, and X. H. Chen, Phys. Rev. Lett. **101**, 257003 (2008).

[29] P. Zavalij, W. Bao, X. F. Wang, J. J. Ying, X. H. Chen, D. M. Wang, J. B. He, X. Q. Wang, G. F. Chen, P.-Y. Hsieh, Q. Huang, and M. A. Green, Phys. Rev. B **83**, 132509 (2011).

[30] S. M. Kazakov, A. M. Abakumov, S. Gonzlez, J. M. Perez-Mato, A. V. Ovchinnikov, M. V. Roslova, A. I. Boltalin, I. V. Morozov, E. V. Antipov, and G. V. Tendeloo, Chem Mater. **23**, 4311 (2011).

[31] Y. Texier, J. Deisenhofer, V. Tsurkan, A. Loidl, D. S. Inosov, G. Friemel, and J. Bobroff, Phys. Rev. Lett. **108**, 237002 (2012).

[32] B. Shen, B. Zeng, G. F. Chen, J. B. He, D. M. Wang, H. Yang, and H. H. Wen, Europhys. Lett. **96**, 37010 (2011).

[33] Y. Zhang, L. X. Yang, M. Xu, Z. R. Ye, F. Chen, C. He, H. C. Xu, J. Jiang, B. P. Xie, J. J. Ying, X. F. Wang, X. H. Chen, J. P. Hu, M. Matsunami, S. Kimura, and D. L. Feng, Nat. Mater. **10**, 273 (2011).

[34] T. Berlijn, P. J. Hirschfeld, and W. Ku, Phys. Rev. Lett. **109**, 147003 (2012).

[35] X. Ding, Y. Pan, H. Yang, and H.-H. Wen, Phys. Rev. B **89**, 224515 (2014).

[36] F. Han, B. Shen, Z.-Y. Wang, and H.-H. Wen, Phil. Mag. **92**, 2553 (2012).

[37] H. Ryu, H. Lei, A. I. Frenkel, and C. Petrovic, Phys. Rev. B **85**, 224515 (2012).

[38] D. Shoemaker, D. Y. Chung, H. Claus, M. C. Francisco, S. Avci, A. Llobet, and M. G. Kanatzidis, Phys. Rev. B **86**, 184511 (2012).

[39] D. Louca, K. Park, B. Li, J. Neuefeind, and J. Yan, Sci. Rep. **3**, 2047 (2013).

[40] C. Duan, J. Yang, F. Ye, and D. Louca, J. Sup. Novel Magn. **29**, 663 (2016).

[41] B. H. Toby and T. Egami, Acta Crystallogr. Sec. A **48**, 336 (1992).

[42] D. Louca, K. Horigane, A. Llobet, R. Arita, S. Ji, N. Katayama, S. Konbu, K. Nakamura, T.-Y. Koo, P. Tong, and K. Yamada, Phys. Rev. B **81**, 134524 (2010).